Towards more free-floating model cell membranes: Method development and application to their interaction with nanoparticles

Nariman Yousefi, Andreas Wargenau, Nathalie Tufenkji*

Department of Chemical Engineering, McGill University, Montreal, Quebec, Canada

KEYWORDS: QCM, membrane, supported lipid bilayer, phospholipid, cytotoxicity, nanoparticle

* Corresponding Author. Phone: (514) 398-2999; Fax: (514) 398-6678; E-mail: nathalie.tufenkji@mcgill.ca

Abstract

Identifying the mechanisms of nanoparticle (NP) interactions with cell membranes is key to understanding their potential cytotoxicity and applications as nano-carriers for targeted drug delivery. To elucidate these mechanisms of interaction, supported phospholipid bilayers (SPBs) are commonly used as models of cell membranes. However, SPBs are soft thin films, and, as such, their properties can be significantly affected by the underlying substrate. Free-floating cell membranes would be best modeled by weakly adhered SPB; thus, we propose a method for tailoring the interfacial interaction of an electrically charged SPB-substrate system based on modulations in the solution chemistry. Using the dissipation signal of the quartz crystal microbalance with dissipation monitoring (QCM-D), we show that the method can be used to tailor SPB-substrate interactions without the loss of its structural integrity. To demonstrate the application of the method, SPBs are exposed to cationic and anionic polystyrene latex NPs. These studies reveal that the bilayer response to the modulations in the interfacial interaction with its underlying substrate can be used as a sensitive tool to probe the integrity of SPBs upon exposure to NPs. As expected, anionic NPs tend to impart no significant damage to the anionic bilayers, whereas cationic NPs can be detrimental to bilayer integrity. This is the first report of a QCM-D based method to probe bilayer integrity following exposure to NPs. Importantly, the degree of SPB interaction with its underlying substrate is shown to be a critical factor in the kinetics of bilayer disruption by cationic NPs, whereby weakly adhered bilayers are prone to significantly faster breakup. Since free-floating cell membranes are better represented by a weakly adhered SPB, the results of this work critically influence paradigms in experimental studies involving SPBs as models for cell membranes.

1. Introduction

Upon exposure, many nanoparticles (NPs) can translocate into cells by passing through the cell plasma membrane – a complex array of various lipids, membrane proteins and sterols (such as cholesterol) that separate cell organelles and compartments from their surrounding environment.[1] In many cases, translocation of NPs into the cells poses cytotoxic risk and, is not desirable;[2–9] however, under controlled conditions, this behavior of NPs can be exploited to engineer nano-carriers for targeted drug delivery applications.[10–12] Hence, understanding the criteria that govern the entry of NPs into cells is of great interest.

In recent years, many efforts have been made to elucidate the mechanisms by which NPs cross the plasma membrane and accumulate inside cells.[13–15] However, due to the intrinsic complexity of such membranes, there are multiple hypotheses and a deeper understanding of the subject matter is yet to be developed.[16–19] This has led many researchers to use supported phospholipid bilayers (SPBs) – planar and substrate-supported arrangements of phospholipids – as robust models for studying NP interactions with cell membranes.[17,20–21]

Use of these simple, yet chemically and geometrically relevant model membranes has contributed to our understanding of the interaction mechanisms of NPs as well as various molecules with lipid bilayers.[22–25] For example, studies involving charged bilayers and NPs have shown that the interaction between the two are affected by electrostatic forces, whereby NPs that carry opposite charge to the lipids can have disruptive effects on the bilayers, while NPs which share the same charge-type as bilayers typically do not pose considerable risk to their integrity.[26–28] Other studies with SPBs and NPs of different sizes suggest that small hydrophobic NPs potentially translocate

in between the leaflets of SPBs.[22,24,29–31] Geometry and aspect ratio of NPs have also been shown to play a critical role on their interaction with lipid bilayers; graphene nanosheets were shown to translocate in between the bilayer's proximal and distal leaflets despite their micron-sized lateral dimensions;[32] a phenomenon that was previously shown for spherical particles with an average diameter of less than 8 nm.[30,31]

Although SPBs were demonstrated to be relevant models for cell membranes and many results obtained using the model bilayers mirror those obtained with corresponding cell lines,[33,34] there remain non-negligible discrepancies between the results obtained using SPBs and cultured cells.[17,20] A close inspection of SPBs reveals that they are essentially thin films due to their relatively small thickness (4–5 nm) and large lateral dimensions (typically tens of millimeters).[35] Thus, SPBs are prone to be affected by their underlying substrates; it has been shown that physical properties of SPBs such as gel-to-fluid transition temperature[36] and lateral diffusion of phospholipid molecules[37] are influenced by their supporting substrates. The significant effects of substrate on the mechanical properties of SPBs have also been reported.[38-41] For example, the extent of deformation in a SPB (which could affect its integrity) upon interaction with an external object (such as NPs or macromolecules) is determined by its stiffness, which can be influenced by the degree of interaction of the bilayer with its underlying substrate. Although there are few reports on the effect of substrate properties such as chemical composition, hydrophobicity and roughness on spontaneous formation of SPBs, the effect of substrate interactions of SPBs and their influence on membrane stability have been mostly neglected in studies where SPBs were used as model cell membranes.[42] Accordingly, the effect of substrate interaction on the bilayer response to NPs is

unknown, despite the fact that such interactions would be influenced by the deformation of SPBs which, as described, could be critically affected by substrate-SPB interactions.[39–41]

Two major challenges in studying the substrate interaction of SPBs are (i) developing an *in situ* method to tailor the degree of interfacial interaction, as well as (ii) finding a suitable non-invasive technique to study the 1–2 nm interfacial zone between the substrate and the SPB.[35] The fact that the interaction between electrically charged bilayers and substrates is affected by electrostatic forces can be exploited to tailor their interaction by means of controlling the net charge of only one of the components. For example, the surface charge of an amphoteric metal oxide substrate such as alumina can be tuned by pH variations close to physiological pH values, where most charged phospholipids do not exhibit pH sensitivity.[43,44] This phenomenon can be used as a robust platform to tailor the interfacial interactions of many charged lipid bilayer-substrate systems.

Studying the interfacial zone is a greater challenge due to the fact that many classical surface sensitive techniques used for studying SPBs do not provide direct access to the very thin interfacial zone. In addition to classical surface sensitive techniques, quartz crystal microbalance with dissipation monitoring (QCM-D), an acoustical characterization method for thin films, has been used to study SPBs.[45–50] The QCM-D sensor is comprised of an AT-cut quartz crystal that oscillates at its fundamental and overtone resonance frequencies when an AC current is applied. Deposition of mass (Δm) onto the crystal results in an increase of mass of the resonator and gives rise to negative frequency shifts (Δf). Mass deposition also results in dissipative energy losses in the sensor that are characterized by the oscillation decay time (*i.e.*, dissipation factor, D). For the case where the deposited mass results in the formation of a homogeneous film and the dissipative

energy losses are small ($\Delta D/\Delta f < 10^{-7}$ Hz^{-1} for all overtones), the relationship between adsorbed mass Δm and the induced frequency shift is expressed by the Sauerbrey equation:[51]

$$\Delta m = -\frac{\Delta f_n}{n} \times C \quad (1)$$

where Δf_n is the measured frequency shift at overtone number n and C is the mass sensitivity constant that equals 17.7 ng cm^{-2} Hz^{-1} for a 5 MHz AT-cut crystal.

The frequency shift of QCM-D has been utilized for monitoring deposition of lipid vesicles, their spontaneous collapse into bilayers and their further interactions with NPs.[46–49] However, the complementary dissipation signal (ΔD), which carries valuable information about the interfacial energy loss associated with the deposited mass, has been largely neglected in SPB studies. The dissipation of oscillatory energy is dependent on the coupling of the mass to the sensor surface;[45] thus, QCM dissipation monitoring has the potential to detect the interaction between a SPB and its underlying substrate.[52]

We report a method for tuning the substrate interaction of SPBs by means of modulations in the medium pH. The dissipation signal of QCM-D was used as a sensitive tool to probe the extent of SPB-substrate interfacial interactions. Moreover, the effect of SPB-substrate interactions on the disruptive potential of NPs towards bilayers was investigated using the QCM-D dissipation signal and fluorescence microscopy. This is the first report to demonstrate the effect of SPB-substrate interaction as a major contributor to the response of SPBs towards NPs.

2. Materials and methods

2.1. Preparation of small unilamellar vesicles (SUVs)

Chloroform solutions of 1-palmitoyl-2-oleoyl-sn-glycero-3-phosphoethanolamine (POPE, Avanti Polar Lipids) and 1-palmitoyl-2-oleoyl-sn-glycero-3-phospho-(1'-rac-glycerol) (POPG, Avanti Polar Lipids) were mixed at a ratio of POPE:POPG 1:2 in a glass culture tube and dried under a stream of high-purity nitrogen. The resulting film was then desiccated under vacuum for 2 h to remove any residual organic solvents. Dried lipids were then hydrated with a 10 mM Tris (Tris(hydroxymethyl)aminomethane, Sigma Aldrich) buffer (pH 7.5) containing 100 mM sodium chloride (NaCl, Fisher) for 40 min with intermittent vortexing to obtain large multilamellar vesicles (LMVs). SUVs were prepared through successive extrusion of the LMV suspension against polycarbonate membranes (PC membranes, Avanti Polar Lipids) with average pore sizes of 0.1 and 0.03 μm, respectively. The dispersions were extruded 11 times against each of the membranes to ensure that mono-disperse SUVs with average diameter of approximately 30 nm were obtained. The final phospholipid concentration was 1 mg/mL.

2.2.Real-time monitoring of SPB formation and NP deposition using QCM-D

Bilayer formation and NP deposition were studied using a QCM-D (Q-Sense E4, Biolin Scientific). All experiments were performed using aluminum oxide coated sensors (Biolin Scientific) that were washed thoroughly with deionized (DI) water, dried under a stream of high-purity nitrogen and treated in a UV/ozone chamber (Bioforce Nanosciences) for 20 min prior to each experiment. In a typical experiment, sensors were rinsed with 10 mM Tris buffer (pH 7.5) for 15 min followed by a rinse with SUV dispersions (0.1 mg/mL) until the frequency and dissipation shift values stabilized at approximately –26 Hz and less than 0.2×10^{-6}, respectively. Due to large signal to noise ratio, the frequency and dissipation shifts reported are from the 3rd overtone, unless otherwise

stated. For pH modulation experiments, the pH of 10 mM Tris buffers containing no sodium chloride were adjusted to pH 7.0, 7.5, 8.0, and 8.5 using 1 M HCl. In a typical pH modulation experiment, the SPB or SPB-NP hybrid was successively rinsed with each of the above buffers for 10 min. A final rinse using pH 7.0 buffer was performed to evaluate the reversibility of the pH modulation procedure.

Polystyrene latex nanoparticles with carboxyl (carboxyl latex beads, 0.02 μm, Invitrogen Life Technologies) and amidine (amidine latex beads, 0.02 μm, Invitrogen Life Technologies) surface functional groups were used as model NPs. Latex NPs were diluted to a concentration of approximately 0.04 mg/mL (approximately 10^{12} particles/mL) using 10 mM Tris buffer (pH 7.0) containing no sodium chloride and sonicated for 20 min in a bath sonicator (FS60H, Fisher Scientific) prior to deposition on SPBs. The bilayers were exposed to NPs at a flow rate of 0.2 mL/min for at least 60 min, unless otherwise stated. The corresponding Peclet number was 5.45×10^{-6} confirming that NP deposition was diffusion controlled.

After each experiment, the crystals were cleaned by 30 min sonication in 1% Hellmanex (Hellmanex III, Hellma) solution, were subsequently rinsed with ethanol and DI water, dried under a stream of nitrogen and were finally treated with UV/ozone for 30 min.

2.3.Characterization of NPs and SUVs

Hydrodynamic diameter of SUVs and NPs was measured by dynamic light scattering (DLS, ZetaSizer Nano ZS, Malvern Instruments). Electrophoretic mobilities of the SUVs and NPs were measured by laser Doppler micro-electrophoresis (ZetaSizer Nano ZS, Malvern Instruments). DLS

and electrophoretic mobility measurements were conducted using at least three independent samples.

2.4. Imaging of SPBs

For fluorescence microscopy, 2 wt% of fluorescent-tagged 1-myristoyl-2-{6-[(7-nitro-2-1,3-benzoxadiazol-4-yl)amino]hexanoyl}-sn-glycero-3-phosphocholine (Avanti Polar Lipids) was added to the POPE:POPG mixture prior to the drying step to obtain fluorescent lipid mixtures. QCM-D crystals were carefully removed from the fluid chambers while in continuous contact with Tris buffer to avoid exposure of the lipids to air. Fluorescence microscopy images of SPB-coated QCM-D crystals were taken at a magnification of 200× using an Inverted Fluorescence Microscope (IX71, Olympus) equipped with a FITC filter cube (U-N31001, Chroma) with excitation and emission wavelength ranges of 465–495 and 515–550 nm, respectively. The images were analyzed using ImageJ software (National Institute of Health) to determine the surface area of fluorescent patches which we defined as the percentage of green pixels among total pixels in an image. At least 5 images were analyzed in each case and the average and the standard deviation of the obtained fluorescence values were determined.

3. Results and discussion

3.1. Development of a method for the preparation of more free-floating SPBs

Upon exposure to the positively charged alumina substrate, small unilamellar vesicles (SUVs) of POPE:POPG lipid mixtures suspended in 10 mM Tris at pH 7.5 (containing 100 mM NaCl) quickly adsorb to the surface, giving rise to a large QCM-D frequency shift (~ –30 Hz). When the surface is covered by sufficiently large number of SUVs, they spontaneously collapse to form

planar SPBs, as evidenced by the distinctive increase in frequency caused by release of entrapped water, followed by stabilization of the frequency and dissipation shifts at final values of –26 ± 0.8 Hz and 0.1 ± 0.04 $\times 10^{-6}$ units, respectively. Such low dissipation shifts are typically reported for rigid homogeneous SPBs (Fig. 1).[45]

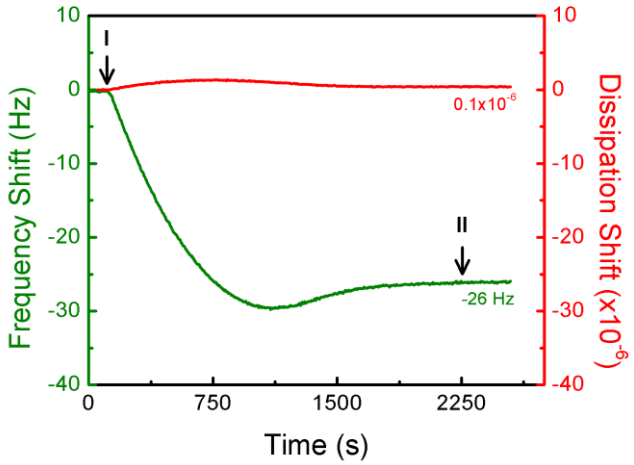

Figure 1. Vesicles of a 1:2 POPE:POPG mixture readily formed homogeneous SPB films upon deposition onto an alumina surface at pH 7.5 as evidenced by the QCM-D frequency and dissipation shifts (the arrow at I denotes start of SUV injection and the arrow at II indicates the start of a buffer rinse).

The interfacial interaction of the SPB with the alumina substrate was studied using the QCM-D dissipation signal (Fig. 2). The dissipation of energy in the QCM-D sensor correlates with the mechanical and dampening properties of the deposited mass, as well as its degree of coupling (adhesion) to the oscillating surface.[45] The interface is the critical point for transfer of oscillation from the sensor to the deposited film; in an ideal case, a deposited homogeneous mass such as a SPB that fully couples (adheres) to the sensor surface (albeit separated from the substrate by a 1–2 nm interfacial water layer),[35] oscillates in phase with the substrate. In fact, there is little

dissipation shift observed following the deposition of SPB (e.g., $\Delta D < 0.2\times10^{-6}$). In contrast, a weaker interface results in an out-of-phase oscillation between the SPB and the substrate; part of the mechanical energy is dissipated, for instance through the "slipping" of the weakly adhered film on the sensor surface, giving rise to a higher dissipation than the case of a well-bonded SPB.[52]

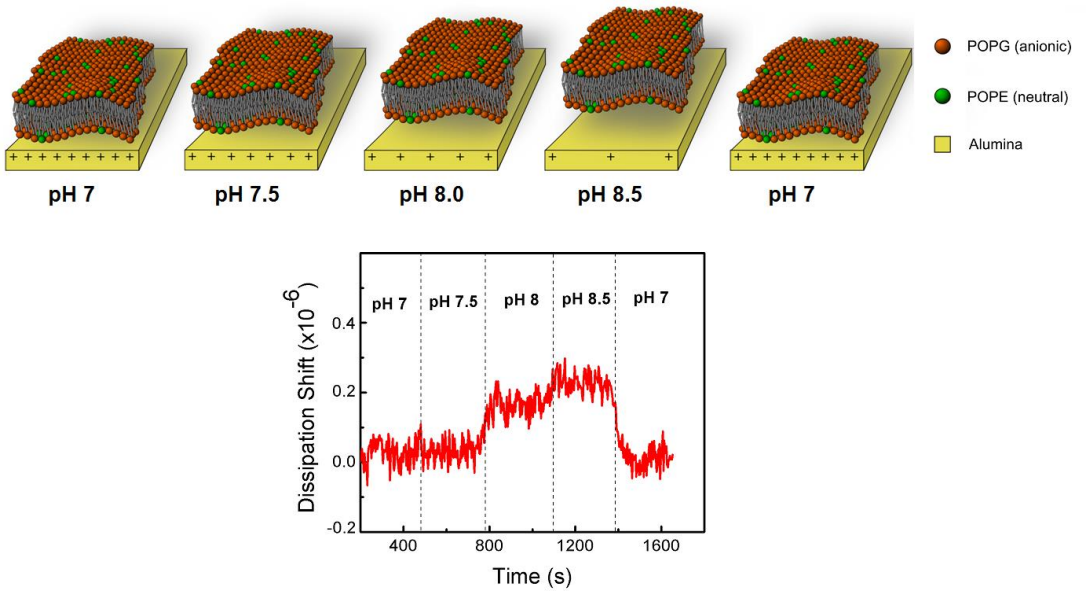

Figure 2. QCM-D dissipation response due to the variations in the degree of interfacial interaction between the amphoteric alumina substrate and the 1:2 POPE:POPG SPB at different medium pHs. The schematic representation of the SPB is not drawn to scale; the gap between the bilayer and the substrate is exaggerated for clarity.

The amphoteric nature of the alumina substrate is key to tailoring the interfacial interaction between the lipid bilayer and the substrate. The surface charge of the amphoteric alumina substrate can be tuned by varying the medium pH,[53] while the overall electric charge of the lipid mixture does not show relevant dependence on the solution chemistry (Table 1). The isoelectric point of alumina-coated QCM-D sensor is reported to be 8.7,[54] hence an increase of pH from 7.0 to 8.5

renders the surface of alumina less positively charged, which in turn, translates to lower electrostatic attraction between the substrate and the SPB at higher pH values. In addition, the elevated sensitivity of alumina at near neutral pH makes it a suitable substrate for model experiments at physiological pH values. It is noteworthy that the decrease in the interfacial interaction of the substrate and the bilayer only leads to a slight increase in the distance between the two, and, even at pH 8.5, the bilayer is still adhered to the substrate, otherwise it would be convected away under the flow.

Table 1. Effect of pH on the electrophoretic mobility of lipid vesicles

Material	pH	Electrophoretic mobility (μm.cm/V.s)
1:2 POPE:POPG SUVs		
	7.0	–1.21 ± 0.13
	7.5	–1.18 ± 0.14
	8.0	–1.16 ± 0.13
	8.5	–1.25 ± 0.11

Interestingly, the pH response of the SPB-substrate system was fully reversible; ΔD increased from 0 to about $0.20 \pm 0.09 \times 10^{-6}$ when the pH was shifted from 7.5 to 8.0, then 8.5 and returned back to its original value when the pH was shifted back to 7 (Fig. 2). This recovery in ΔD is a testament to the fact that reversible electrostatic interactions prevail in the charged substrate-SPB system. Furthermore, modulation of the pH in this range does not impart damage to the bilayer; otherwise, a non-reversible dissipation shift would be expected at the final rinse with pH 7 buffer (Fig. 2).

To prove that the developed technique can be applied to different SPBs, the pH modulation-based tuning of the interfacial attraction was also performed on a different charged lipid mixture; namely,

1,2-dimyristoyl-sn-glycero-3-phosphoethanolamine (DMPE) and 1,2-dimyristoyl-sn-glycero-3-phospho-(1'-rac-glycerol) (DMPG). Unlike POPE and POPG, DMPE and DMPG are saturated phospholipids and the transition temperature of their mixture is above room temperature (up to 50 °C).[55] Interestingly, it was observed that, at room temperature, the gel phase SPBs of DMPE:DMPG are more sensitive to the medium pH modulation in comparison to their fluid phase counterparts of POPE:POPG (Fig. S1). DMPE and DMPG lipids share the same head groups as POPE and POPG, respectively; hence their electric charges are comparable. However, the size of their tail groups is different. Since both DMPE:DMPG and POPE:POPG mixtures are electrostatically equivalent, POPE:POPG mixture was chosen for this study due to the greater biological relevance of fluid lipids at ambient conditions.

A study on the effect of net electric charge of lipid mixtures on their pH responsiveness was also performed (Fig. S1). It was established that for the lipid mixture to be responsive to the pH modulation-based interfacial interactions, it should carry sufficient net negative charge; a composition containing less DMPG lipid than a 1:1 mixture of DMPE:DMPG was found to be insensitive to pH changes (Fig. S1). Preliminary experiments revealed that use of higher amounts of negatively charged POPG lipid resulted in incomplete formation of bilayers (data not shown); thus, POPE:POPG mixtures possessing greater net negative charge were not further investigated and 1:2 POPE:POPG mixtures were chosen as model membranes for the rest of this study.

The results in Figs. 2 and S1 show that we developed a simple QCM-D based method to (i) tailor the interaction between the lipid bilayer and the underlying substrate, and (ii) to indirectly monitor

the integrity of the SPB by observing changes in the dissipation shift during modulation of the medium pH.

3.2. Application of the QCM-D method to study the effect of NP charge on bilayer integrity

Multiple studies report on the membrane disruptive behavior of NPs that carry an opposite electric charge to that of the bilayer and the benign nature of NPs that carry the same charge type as the SPBs they interact with.[27,28,55] To further understand the interaction of charged NPs and bilayers as well as possible NP disruptive effects or mechanisms of entry, the negatively charged 1:2 POPE:POPG SPBs were exposed to 20 nm negatively or positively charged polystyrene latex NPs.

QCM-D studies involving NP interaction with SPBs are often limited by comparatively large frequency shifts during NP deposition.[56,57] When compared with the characteristic frequency shift during bilayer formation, a large Δf due to NP deposition makes detection of less sensitive phenomena such as hole formation and partial bilayer disruption difficult, and often, secondary surface sensitive techniques such as atomic force microscopy (AFM) and surface plasmon resonance (SPR) are needed to confirm the mechanism of interaction. However, formation of holes and partial bilayer disruption are phenomena that can significantly affect the substrate interaction of SPBs; hence, they are expected to be detectable with a sufficiently sensitive interfacial probing method. The developed method for investigating the interfacial interaction of SPBs by monitoring the dissipation response of QCM-D to pH modulation is a good candidate to investigate SPB interactions with NPs.

Exposure of the negatively-charged SPB to negatively-charged carboxyl latex NPs resulted in a frequency shift of –20 ± 1.7 Hz (equivalent to 3.7×10^{10} particles per cm^2 or ~12 % surface coverage), despite the fact that both NPs and the SPB carried a net negative charge (Fig. 3a). For comparison, control experiments were conducted to examine deposition of carboxyl latex NPs on the bare alumina crystal (Fig. S2a). These experiments showed that carboxyl latex NPs readily deposit on the alumina surface, giving rise to a frequency shift of approximately –136 ± 1.9 Hz, which corresponds to a theoretical surface coverage of ~82 %.

The SPB-NP hybrid was subjected to pH modulation to probe its interactions with the underlying substrate (Fig. 3b). The dissipation response of the SPB-NP hybrid corresponded well to that of an intact bare bilayer (Fig. 2), suggesting that the bilayer remained unaffected to a large degree. Interestingly, the absolute dissipation shifts of the hybrid at pH 8 and 8.5 (Fig. 3b) are higher than those measured for the bare bilayer (Fig. 2). This is likely due to the presence of discrete NPs deposited on the bilayer that further contribute to the dissipation of oscillatory energy by acting as individual resonators (Fig 3c).[45] In addition, an increase in pH results in a decrease in the charge of the alumina substrate, leading to the weakening of the electrostatic attraction between the positively charged alumina and the negatively charged carboxyl NPs. Consequently, the contribution of each individual NP to the energy dissipation of the QCM-D is expected to increase with increasing pH.[45]

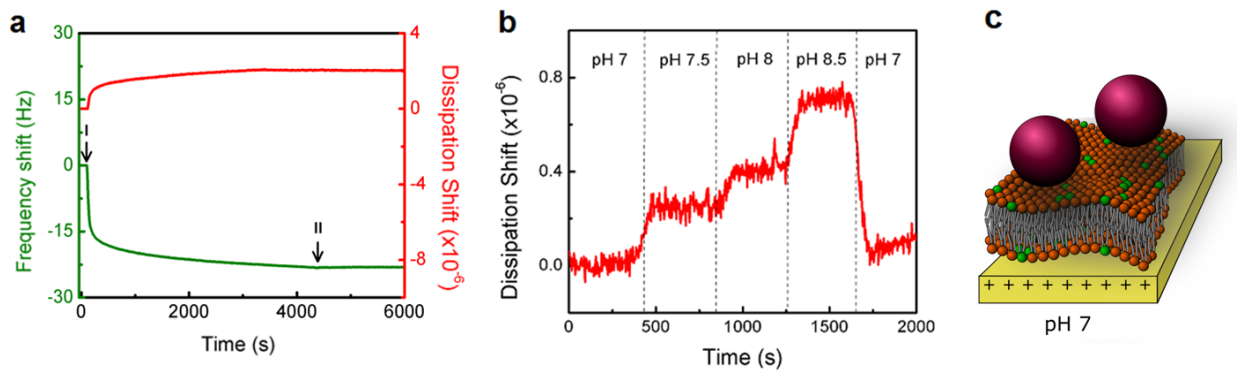

Figure 3. (a) QCM-D measurements during deposition of carboxyl latex NPs on 1:2 POPE:POPG SPB at pH 7 (the arrow at I denotes start of NP injection and the arrow at II indicates the start of a buffer rinse), (b) the pH response of the SPB-NP hybrid, and (c) schematic representation of carboxyl NP deposition on the SPB (not drawn to scale).

Inspection of Fig. 3b reveals a slight difference between the dissipation shift at the initial and final rinses of the SPB-NP hybrid with pH 7 buffer. This can be attributed to slight damage imparted by the NPs to the supported bilayer; nonetheless, the bilayer was largely intact as it responded as expected to pH shifts. This result is in agreement with observations made using other techniques such as AFM and confocal microscopy on giant unilamellar vesicles that highlight how anionic NPs generally have a non-disruptive interaction with anionic lipid bilayers.[1,7,28]

A remarkably different deposition behavior was observed when the negatively-charged SPBs were exposed to positively-charged amidine latex NPs. The NPs deposited extensively on the SPB, rapidly reaching an initial saturation plateau (point 2 in Fig. 4a; equivalent to 2.25×10^{11} particles per cm^2 or 68% surface coverage). Due to geometrical constraint for a closed packed arrangement of spherical NPs, a maximum surface coverage of 74% can be attained; thus, the calculated surface

coverage of 68% at the 1st plateau translates into a near complete monolayer coverage of the SPB with amidine NPs.

Continued exposure to the NPs triggered a second deposition phase where an approximately 5-fold frequency shift was observed until a secondary saturation plateau was reached (point 6 in Fig. 4a). The frequency shift at the second plateau is equivalent to 1.04×10^{12} particles per cm^2 or ~4.5 times more deposition than a monolayer coverage which suggests clumping of the NP-SPB hybrid at the alumina surface. The dual deposition regime and the duration of the transition phase between the 1st and 2nd plateaus was reproducible which is indicative of a systematic process (Fig. 4b). The dual deposition plateau was observed at all overtones (Fig. S3). This dual deposition regime was not observed for carboxyl NPs, even after prolonged exposure of the bilayer to NPs (Fig. 3a).

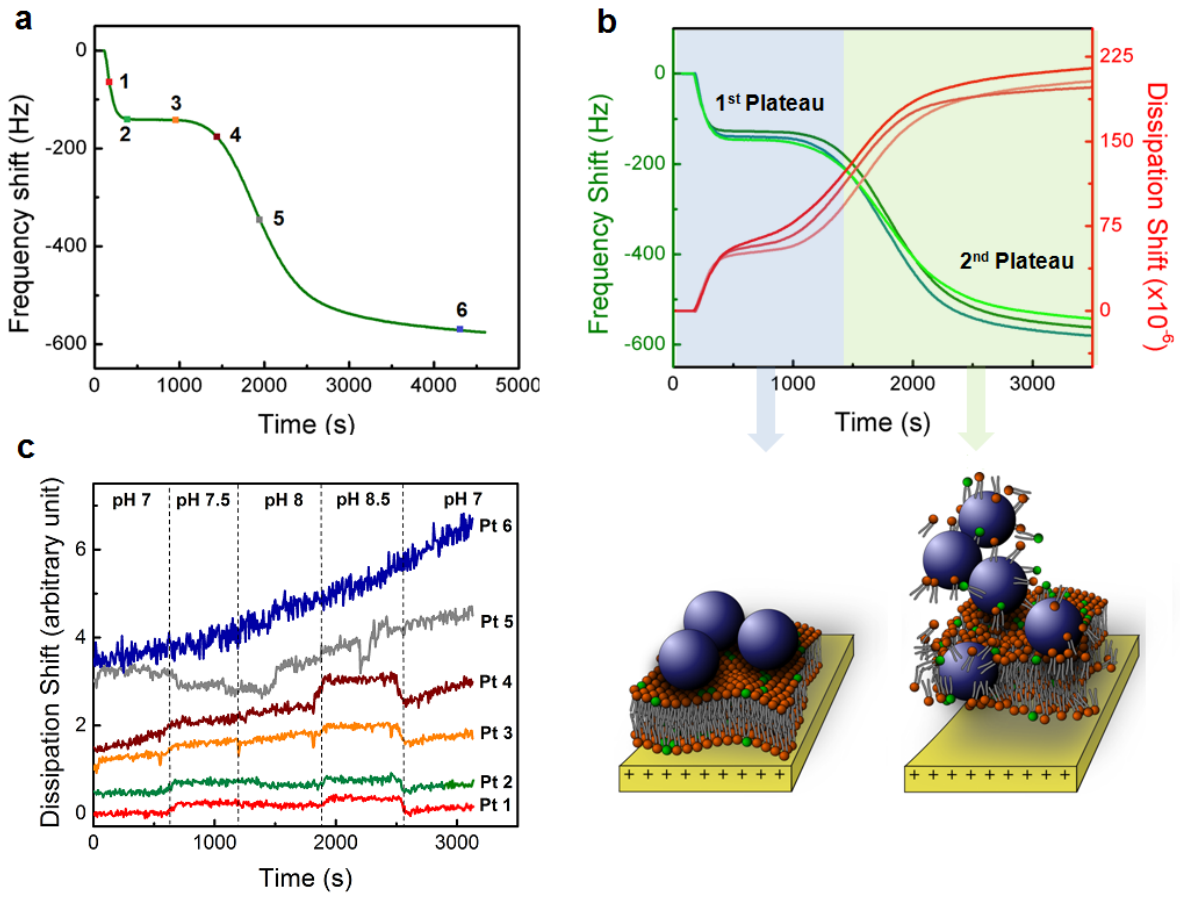

Figure 4. (a) Deposition of amidine latex NPs on 1:2 POPE:POPG SPBs at pH 7 resulted in a dual plateau deposition regime. (b) Three representative curves from replicate experiments are shown to demonstrate the reproducibility of the technique. (c) pH modulation at six successive time points of the NP deposition profile demonstrates that the bilayers were mostly intact at the first plateau while continued exposure to NPs resulted in bilayer disruption, as shown schematically in (b).

It is important to note that the frequency shift due to the deposition of amidine latex NPs is too large (~ –600 Hz) to resolve a few Hz of frequency shift resulting from events such as hole formation or even full bilayer disruption scenarios. To better understand the dual plateau deposition, the QCM-D experiment was repeated 6 separate times and stopped at 6 distinct time-points at which, the formed SPB-NP hybrids were subjected to pH modulations (Fig. 4c). The pH

modulations were performed in the same manner as for the SPB-NP hybrids obtained with carboxyl latex NPs (Fig. 3b). The responses of the SPB-NP hybrids to pH modulation at points 1 and 2 were very similar to those of an intact bilayer; namely, the dissipation shift returned to its original value when the pH was changed to the initial value (pH 7.0) (Fig. 4c). This leads to the conclusion that the SPB at the first plateau is mostly intact. At point 3, the dissipation does not fully return to the original starting value when the pH is decreased to 7.0. This suggests that the bilayer has suffered some initial damage. Starting from point 4, which corresponds to the onset of the second deposition phase, the response of the SPB-NP hybrid to pH modulation began to change considerably. A noticeable difference can be observed between the dissipation at initial and final rinses with pH 7.0 buffer. This observation is a reflection of a damaged bilayer. At point 5 – the midpoint of the second deposition phase – the pH response was entirely irreversible, and at point 6 which coincides with the second plateau, the pH response was completely lost and a constantly increasing drift in dissipation was observed.

The gradual change in the pH response of the SPB-NP hybrid at different stages of amidine NP deposition is indicative of a kinetic process whereby NPs initially deposit on the bilayer without inducing major disruption or damage. When the hybrid is further exposed to the oppositely charged NPs, the bilayer integrity is lost in a time-dependent manner until the bilayer is completely damaged (Fig. 4b). It is hypothesized that at the second plateau, the once distinctively layered hybrids transformed into large aggregates of disassembled lipids and NPs, as evidenced by the remarkably high frequency and dissipation shifts at point 6. In particular, the exceptionally large dissipation shift at the second plateau is characteristic of the deposition of large discrete objects, which typically give rise to greater dissipative energy losses.[46] Since amidine latex NPs and SPBs

attract each other electrostatically and show an affinity to the alumina substrate (see Fig. S2b for amidine latex NP deposition on bare alumina crystal), these aggregates adhered well to the crystal surface and were not washed out throughout the experiment, as evidenced by a lack of positive frequency shift in Fig. 4b.

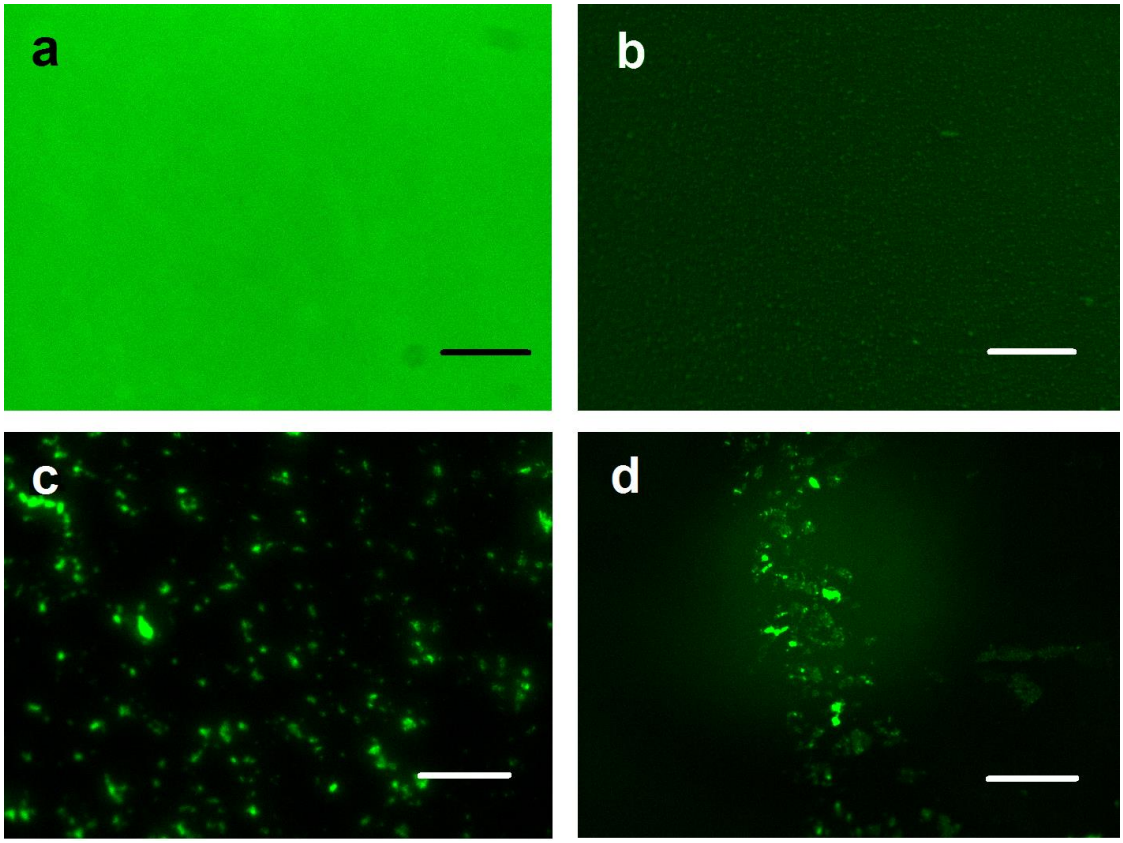

Figure 5. Fluorescence microscopy of (a) the bare SPB, and (b) SPB-NP hybrid at deposition point 3 revealed a uniform deposition of NPs on top of the lipid bilayer. The SPB-NP hybrids at deposition point 6 showed (c–d) a high density of damaged patch formation. The scale bars in all images represent 50 μm.

To further support the above hypothesis, the SPB-NP hybrids at the first (point 3) and second plateaus (point 6) were investigated using fluorescence microscopy. The entire QCM-D

experiment was repeated with fluorescent SUVs formed by adding 2 wt% of a fluorescently-tagged lipid to the 1:2 POPE:POPG mixture. Adding the fluorescently-tagged lipid did not affect the SPB formation, its pH responsiveness and NP deposition onto it (Fig. S4). Additionally, in agreement with the QCM-D dissipation results of Fig. 2, changing the pH did not result in any observable damage to the bilayers (Fig. S5). The fluorescence intensity of the bilayer decreased after depositing the NPs onto the SPB (Fig. 5a and b). Polystyrene latex has been reported to be a fluorescence quencher and the decrease of fluorescence intensity could be attributed to the quenching effect of the NPs.[58,59] The SPB-NP hybrids corresponding to the first plateau were mostly homogeneous (Fig. 5b). However, the fluorescence microscopy of SPB-NP hybrids at the second plateau revealed irregularities in the form of highly fluorescent patches scattered among a dark background (Fig. 5c,d). Quantitative image analysis of the images taken at the second plateau (Fig. 5c,d) revealed that the surface coverage by fluorescent patches (determined by the percentage of the green pixels among total pixels) was 26.4 ± 8.7 %. The highly fluorescent areas in Fig. 5c and 5d are likely due to bilayer damage, where NPs no longer form a uniform and homogeneous layer atop the SPB. When compared to Fig. 5b at the first plateau, it can be hypothesized that the SPB-NP hybrid at the second plateau (Fig. 5c,d) was comprised of patches of fluorescent lipids and non-fluorescent NPs, suggesting a damaged bilayer. The extent of damage was diverse, including almost uniformly distributed patches (Fig. 5c), and more localized areas of damage (Fig. 5d), suggesting disruption and irregular mixing of NPs and SPB components, that resulted in the displacement of the fluorescent lipids from the layer below the NPs to the top of the disrupted mixture. This bilayer damage coincides with the deterioration of the dissipation shift during pH modulation.

Based on the QCM-D nanoparticle deposition profiles, the results of pH modulation experiments on SPB-NP hybrids, and the fluorescence microscopy observations, a likely mechanism of interaction can be formulated. According to the observations, amidine latex NPs initially deposited on the oppositely charged SPB with negligible impact on bilayer integrity; however, with further exposure to the NPs, damage (such as holes) was induced in the bilayer and displaced sections of the SPBs further interacted with the freshly introduced NPs. The secondary interaction of the disrupted bilayer and NPs resulted in a second deposition instance, where additional damage was imparted and as a result, more NPs were deposited until the high density of damaged patches gave rise to an irregular mixture of disrupted bilayers and NPs, which is coincident with reaching the second plateau (Fig. 4b). Bilayer disruption through hole "nucleation and growth" has also been reported in a recent AFM study, showing how negatively charged gold NPs induced holes in a positively charged bilayer and continued exposure to NPs for up to one hour resulted in hole growth and extensive bilayer disruption.[60] Complimentary to AFM, the sensitive QCM-D based method reported herein provides the advantage of real-time monitoring, and hence enables the characterization of bilayer disruption kinetics.

It is important to note that the above phenomena could not be resolved by reliance on only the QCM-D frequency and dissipation shifts observed during deposition of the NPs (Fig. 4a). These results show that the capability of probing the bilayer response to interfacial interactions with the facile and rapid QCM-D method of pH modulation (Fig. 4c) was key to understanding the mechanism of interaction of cationic amidine latex NPs with the SPB.

3.3. Application of the QCM-D method to examine the influence of substrate-bilayer interactions on bilayer disruption

Having confirmed the interaction of amidine latex NPs with the 1:2 POPE:POPG SPB, it is of interest to investigate whether the degree of interaction of the SPB with the underlying substrate can affect the disruptive behavior of the amidine NPs. The data presented in the previous section corresponds to NP deposition at pH 7. In this section, we discuss NP deposition at higher pH values, where the electrostatic attraction between the SPB and the substrate is expected to be weaker (Fig. 2).

The charge of the alumina substrate becomes less positive with increasing pH; thus, the interaction strength between the substrate and the 1:2 POPE:POPG SPB will decrease with increasing pH from 7 to 8.5 (Fig. 2). Amidine latex NPs were deposited on SPBs that had been equilibrated at higher pH values (Fig. 6a). Decreasing the substrate interaction of the SPB considerably influenced how it interacted with NPs. Firstly, the initial deposition rate of the amidine latex NPs (*i.e.*, the slope of the frequency and dissipation shift profiles at the onset of initial deposition in the first phase) increased as the interfacial interaction of the bilayer with the underlying substrate became weaker (Fig. 6b, c and Table 2).

Table 2. Deposition rates of amidine NPs at the first and second plateau

pH	Deposition rate at 1st plateau (Hz/s)	Deposition rate at 2nd plateau (Hz/s)

7.0	–1.29 ± 0.21	–0.52 ± 0.07
7.5	–1.41 ± 0.27	–0.53 ± 0.1
8.0	–1.46 ± 0.14	–0.60 ± 0.03
8.5	–1.87 ± 0.31	–0.62 ± 0.13

It is important to note that the physicochemical properties (*i.e.*, zeta potential and hydrodynamic diameter) of the amidine latex NPs and the net charge of phospholipids (*i.e.*, zeta potential of SUVs) did not change significantly over the tested pH range (Table 3). In other words, changing pH did not cause a major change in the surface charge of the NPs, nor did it result in their aggregation. Thus, the observed "apparent" increase in the rate of NP deposition onto the SPB can be directly attributed to the weaker interaction of the SPB with its underlying substrate. Another important effect of the weaker interfacial SPB-substrate interaction is the fact that the transition from the first deposition plateau to the secondary deposition phase – an indicator of bilayer damage – occurred considerably earlier. Accordingly, the results in Fig. 6 show that substrate interaction of SPBs is a key factor that determines their resistance to bilayer damage (and disruption) in the event of exposure to NPs.

Table 3. Effect of pH on electrophoretic mobility and hydrodynamic diameter of amidine NPs

Material	pH	Electrophoretic mobility (µm.cm/V.s)	Average diameter (nm)
Amidine latex NPs			
	7.0	0.95 ± 0.03	26.3 ± 1.3
	7.5	1.05 ± 0.06	25.4 ± 1.6
	8.0	1.03 ± 0.06	25.5 ± 0.8
	8.5	0.90 ± 0.08	23.5 ± 1.1

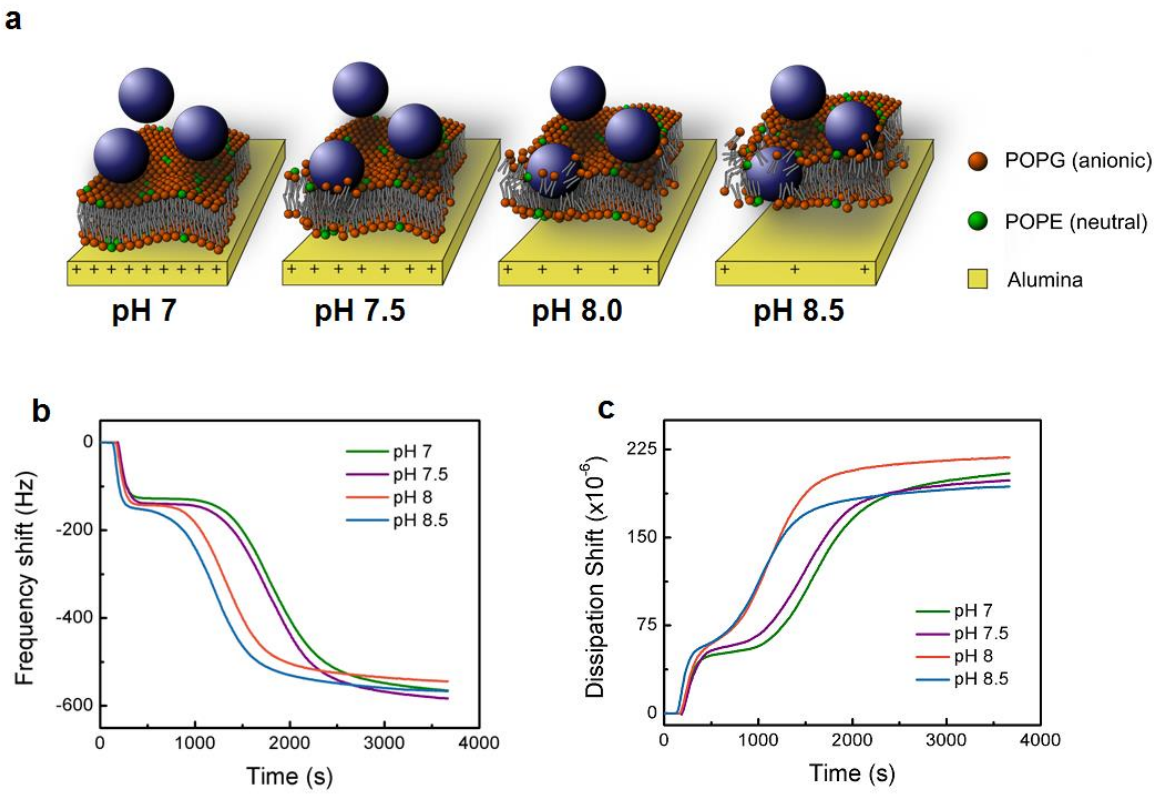

Figure 6. (a) Schematic representation of amidine latex NP deposition onto a SPB formed on alumina at different pH values (not to scale) and (b) QCM-D frequency and, (c) dissipation shifts during deposition of amidine latex NPs at different pHs.

If SPBs are to be used as realistic model membranes for studies on NP cytoxicity or NP-enabled drug delivery, their interaction with the underlying substrate must be taken into account. This critical factor has been neglected in studies involving SPBs and could be one of the key reasons behind observed discrepancies between studies involving cultured cells and their relevant SPBs.[17,20] Based on our findings, to mimic the conditions experienced by free-floating cell membranes, it is best to conduct SPB studies at conditions that lead to weaker substrate-SPB interactions. Thus, the demonstrated substrate effects on bilayer disruption can critically influence the paradigms in experimental studies involving SPBs as models for cell membranes.

4. Conclusions

In an effort to form a SPB that better mimics a free-floating membrane, we proposed a method to assess the interaction between a charged SPB with the underlying substrate by controlling their electrostatic attraction and monitoring its energy dissipation by QCM-D. Weaker interfacial interactions between a charged SPB and an alumina substrate induced by modulating the medium pH led to a more free-floating SPB, characterized using the dissipation signal of a QCM-D. In the second part of this study, we showed that analyzing the interfacial response of the SPB to pH modulation can be a powerful tool to probe the integrity of bilayers upon their interaction with positively- and negatively-charged latex NPs. While negatively-charged carboxyl latex NPs did not impart damage to bilayers, positively-charged amidine latex NPs disrupted SPBs through a two-stage kinetic process where NPs initially deposited on the SPB but imparted damage to the bilayer through continued exposure by formation of localized damaged patches and their coalescence. Furthermore, the interaction of SPBs with the underlying substrate was shown to be a key factor in determining the transition from the first phase of amidine NP deposition to the second deposition/disruption phase, whereby a weaker interaction led to a faster transition to the disruptive phase. These findings suggest that substrate-bilayer interaction of SPBs affect their integrity upon NP deposition and, therefore, this interaction should be considered if SPBs are to be used as models for cell membranes. Since a SPB with weaker substrate interaction better models a free-floating membrane, the proposed method can be very useful in the design of future studies probing the interaction of NPs, toxins, proteins or contaminants with SPBs. Thus, the proposed QCM-D method can be useful to support fundamental studies with applications in nano-cytotoxicity studies, drug delivery, and toxicology.

Acknowledgements

This project was funded by a Natural Sciences and Engineering Research Council of Canada Discovery grant to N.T., a Canada Research Chair grant to N.T., the NSERC CREATE Research and Training via the Institute in Water, Energy and Sustainability Systems (414198-2012), and the Ministère du Développement économique, Innovation et Exportation (MDEIE) PSR-SIIRI program. The authors thank Nicholas Lin for preparing the lipid bilayer graphics.

Supporting Information Available: QCM-D experimental results for SPBs formed using different mixtures of DMPE:DMPG, deposition profile of amidine NP on SPBs shown at all overtones, control deposition of amidine and carboxyl NPs on alumina surface, formation of fluorescent SPBs on alumina and the effect of medium pH on the integrity of fluorescent SPBs. These materials are available free of charge via the Internet at http://pubs.acs.org.

References

(1) Leroueil, P. R.; Hong, S. P.; Mecke, A.; Baker, J. R.; Orr, B. G.; Holl, M. M. B. Nanoparticle Interaction with Biological Membranes: Does Nanotechnology Present a Janus Face? *Acc. Chem. Res.* **2007**, *40*, 335–342.
(2) Hong, S.; Hessler, J. A.; Banaszak Holl, M. M.; Leroueil, P. R.; Mecke, A.; Orr, B. G. Physical Interactions of Nanoparticles with Biological Membranes: The Observation of Nanoscale Hole Formation. *Chem. Health Saf.* **2006**, *13*, 16–20.
(3) Borm, P. J. A.; Kreyling, W. Toxicological Hazards of Inhaled Nanoparticles - Potential Implications for Drug Delivery. *J. Nanosci. Nanotechnol.* **2004**, *4*, 521–531.
(4) Donaldson, K.; Stone, V.; Tran, C. L.; Kreyling, W.; Borm, P. J. A. Nanotoxicology. *J. Occup. Environ. Med.* **2004**, *61*, 727–728.
(5) Duncan, R.; Izzo, L. Dendrimer Biocompatibility and Toxicity. *Adv. Drug Delivery Rev.* **2005**, *57*, 2215–2237.
(6) Oberdorster, G.; Oberdorster, E.; Oberdorster, J. Nanotoxicology: An Emerging Discipline Evolving from Studies of Ultrafine Particles. *Environ. Health Perspect.* **2005**, *113*, 823–839
(7) Nel, A.; Xia, T.; Madler, L.; Li, N. Toxic Potential of Materials at the Nano Level. *Science* **2006**, *311*, 622–627.
(8) Hoet, P. H. M.; Nemmar, A.; Nemery, B. Health Impact of Nanomaterials. *Nat. Biotechnol.* **2004**, *22*, 19.
(9) Hoet, P. H. M.; Bruske-Hohlfeld, I.; Salata, O. V. Nanoparticles – Known and Unknown Health Risks. *J. Nanobiotechnol.* **2004**, *2*, 12.
(10) Popielarski, S. R.; Pun, S. H.; Davis, M. E. A Nanoparticle-based Model Delivery System to Guide the Rational Design of Gene Delivery to the Liver. 1. Synthesis and Characterization. *Bioconjugate Chem.* **2005**, *16*, 1063–1070.
(11) Bielinska, A. U.; Yen, A.; Wu, H. L.; Zahos, K. M.; Sun, R.; Weiner, N. D.; Baker, J. R.; Roessler, B. J. Application of Membrane-based Dendrimer/DNA Complexes for Solid Phase Transfection in vitro and in vivo. *Biomaterials* **2000**, *21*, 877–887.
(12) Hosseinidoust, Z.; Allam, N.; Sim, G.; Tufenkji, N.; van de Ven, T. G. Cellulose Nanocrystals with Tunable Surface Charge for Nanomedicine. *Nanoscale* **2015**, *7*, 16647–16657.
(13) Verma, A.; Stellacci, F. Effect of Surface Properties on Nanoparticle–Cell Interactions. *Small* **2010**, *6*, 12–21.
(14) Unfried, K.; Albrecht, C.; Klotz, L. O.; Von Mikecz, A.; Grether-Beck, S.; Schins, R. P. Cellular Responses to Nanoparticles: Target Structures and Mechanisms. *Nanotoxicology* **2007**, *1*, 52–71.
(15) Nel, A. E.; Mädler, L.; Velegol, D.; Xia, T.; Hoek, E. M.; Somasundaran, P.; Thompson, M. Understanding Biophysicochemical Interactions at the Nano–Bio Interface. *Nat. Mater.* **2009**, *8*, 543–557.
(16) Lewinski, N.; Colvin, V.; Drezek, R. Cytotoxicity of Nanoparticles. *Small* **2008**, *4*, 26–49.
(17) Chen, K. L.; Bothun, G. D. Nanoparticles Meet Cell Membranes: Probing Nonspecific Interactions Using Model Membranes. *Environ. Sci. Technol.* **2013**, *48*, 873–880.
(18) Guo, D. D.; Wu, C. H.; Li, X. M.; Jiang, H.; Wang, X. M.; Chen, B. A. In Vitro Cellular Uptake and Cytotoxic Effect of Functionalized Nickel Nanoparticles on Leukemia Cancer Cells. *J. Nanosci. Nanotechnol.* **2008**, *8*, 2301–2307.
(19) Ferrari, M. Cancer Nanotechnology: Opportunities and Challenges. *Nat. Rev. Cancer* **2005**, *5*, 161–171.
(20) Edidin, M. Lipids on the Frontier: A Century of Cell Membrane Bilayers. *Nat. Rev. Mol. Cell Biol.* **2003**, *4*, 414–418.
(21) Van Meer, G.; Voelker, D. R.; Feigenson, G. W. Membrane Lipids: Where They are and How They Behave. *Nat. Rev. Mol. Cell Biol.* **2008**, *9*, 112–124.

(22) Gopalakrishnan, G.; Danelon, C.; Izewska, P.; Prummer, M.; Yves Bolinger, P.; Geissbhler, I.; Demurtas, D.; Dubochet J.; Vogel, H. Multifunctional Lipid/Quantum Dot Hybrid Nanocontainers for Controlled Targeting of Live Cells. *Angew. Chem., Int. Ed.* **2006**, *45*, 5478–5483.
(23) Tree-Udom, T.; Seemork, J.; Shigyou, K.; Hamada, T.; Sangphech, N.; Palaga, T.; Wanichwecharungruang, S. Shape Effect on Particle-Lipid Bilayer Membrane Association, Cellular Uptake, and Cytotoxicity. *ACS Appl. Mater. Interfaces* **2015**, *7*, 23993–24000.
(24) Rasch, M. R.; Rossinyol, E.; Huesso, J. L.; Goodfellow, B. W.; Arbiol, J.; Korgel, B. A. Hydrophobic Gold Nanoparticle Self-Assembly with Phosphatidylcholine Lipid: Membrane-loaded and Janus Vesicles. *Nano Lett.* **2010**, *10*, 3733–3739.
(25) Zhang, X. F.; Yang, S. H. Nonspecific Adsorption of Charged Quantum Dots on Supported Zwitterionic Lipid Bilayers: Real-Time Monitoring by Quartz Crystal Microbalance with Dissipation. *Langmuir* **2011**, *27*, 2528–2535.
(26) Cha, T.; Guo, A.; Zhu, X. Y. Formation of Supported Phospholipid Bilayers on Molecular Surfaces: Role of Surface Charge Density and Electrostatic Interaction. *Biophys. J.* **2006**, *90*, 1270–1274.
(27) Lin, J.; Zhang, H.; Chen, Z.; Zheng, Y. Penetration of Lipid Membranes by Gold Nanoparticles: Insights into Cellular Uptake, Cytotoxicity, and Their Relationship. *ACS Nano* **2010**, *4*, 5421–5429.
(28) Li, S.; Malmstadt, N. Deformation and Poration of Lipid Bilayer Membranes by Cationic Nanoparticles. *Soft Matter* **2013**, *9*, 4969–4976.
(29) Chen, Y.; Bose, A.; Bothun, G. D., Controlled Release from Bilayer-decorated Magnetoliposomes via Electromagnetic Heating. *ACS Nano* **2010**, *4*, 3215–3221.
(30) Bothun, G. D. Hydrophobic Silver Nanoparticles Trapped in Lipid Bilayers: Size Distribution, Bilayer Phase Behavior, and Optical Properties. *J. Nanobiotechnol.* **2008**, *6*, 13–23.
(31) Roiter, Y.; Ornatska, M.; Heine, D. R.; Rammohan, A. R.; Minko, S.; Balakrishnan, J. Interaction of Nanoparticles with Lipid Membrane. *Nano Lett.* **2008**, *8*, 941–944.
(32) Titov, A. V.; Král, P.; Pearson, R. Sandwiched Graphene–membrane Superstructures. *ACS Nano* **2009**, *4*, 229–234.
(33) Hong, S.; Leroueil, P. R.; Janus, E. K.; Peters, J. L.; Kober, M. M.; Islam, M. T.; Orr, B. G.; Baker, J. R.; Banaszak Holl, M. M. Interaction of Polycationic Polymers with Supported Lipid Bilayers and Cells: Nanoscale Hole Formation and Enhanced Membrane Permeability. *Bioconjugate Chem.* **2006**, *17*, 728–734.
(34) Sackmann, E. Supported Membranes: Scientific and Practical Applications. *Science* **2006**, *271*, 43–48.
(35) Bayerl, T.M.; Bloom, M. Physical Properties of Single Phospholipid Bilayers Adsorbed to Micro Glass Beads. A New Vesicular Model System Studied by 2H-Nuclear Magnetic Resonance. *Biophys. J.* **1990**, *58*, 357–362.
(36) Seeger, H. M.; Cerbo, A. D.; Alessandrini, A.; Facci, P. Supported Lipid Bilayers on Mica and Silicon Oxide: Comparison of the Main Phase Transition Behavior. *J. Phys. Chem. B* **2010**, *114*, 8926–8933.
(37) Seu, K. J.; Pandey, A. P.; Haque, F.; Proctor, E. A.; Ribbe, A. E.; Hovis, J. S. Effect of Surface Treatment on Diffusion and Domain Formation in Supported Lipid Bilayers. *Biophy. J.* **2007**, *92*, 2445–2450.
(38) Li, Y.; Zhu, C.; Zhu, J.; Liang, H.; Chen, D.; Zhao, H.; Liu, B. Nanomechanics of Phospholipid LB Film Studied Layer by Layer with AFM. *Chem. Cent. J.* **2014**, *8*, 71.
(39) Wang, X.; Sanderson, R. N.; Ragan, R. Evaluation of Young's Modulus of Tethered 1-Palmitoyl-2-oleoyl-sn-glycero-3-phosphocholine Membranes Using Atomic Force Spectroscopy. *J. Phys. Chem. C* **2014**, *118*, 29301–29309.
(40) Wang, H.; Chung, T. S.; Tong, Y. W.; Meier, W.; Chen, Z.; Hong, M.; Armugam, A. Preparation and Characterization of Pore-suspending Biomimetic Membranes Embedded with Aquaporin Z on Carboxylated Polyethylene Glycol Polymer Cushion. *Soft Matter* **2011**, *7*, 7274–7280.

(41) Canale, C.; Jacono, M.; Diaspro, A.; Dante, S. Force Spectroscopy as a Tool to Investigate the Properties of Supported Lipid Membranes. *Microsc. Res. Tech.* **2010**, *73*, 965–972.
(42) Tero, R. Substrate Effects on the Formation Process, Structure and Physicochemical Properties of Supported Lipid Bilayers. *Materials* **2012**, *5*, 2658–2680.
(43) Franks, G. V.; Gan, Y. Charging Behavior at the Alumina–Water Interface and Implications for Ceramic Processing. *J. Am. Ceram. Soc.* **2007**, *90*, 3373–3388.
(44) Shin, Y. J.; Su, C. C.; Shen, Y. H. Dispersion of Aqueous Nano-Sized Alumina Suspensions Using Cationic Polyelectrolyte. *Mater. Res. Bull.* **2006**, *41*, 1964–1971.
(45) Reviakine, I.; Johannsmann, D.; Richter, R. P. Hearing What You Cannot See and Visualizing What You Hear: Interpreting Quartz Crystal Microbalance Data from Solvated Interfaces. *Anal. Chem.* **2011**, *83*, 8838–8848.
(46) Richter, R.; Mukhopadhyay, A.; Brisson, A. Pathways of Lipid Vesicle Deposition on Solid Surfaces: A Combined QCM-D and AFM Study. *Biophys. J.* **2003**, *85*, 3035–3047.
(47) Richter, R. P.; Bérat, R.; Brisson, A. R. Formation of Solid-Supported Lipid Bilayers: An Integrated View. *Langmuir* **2006**, *22*, 3497–3505.
(48) Jackman, J. A.; Tabaei, S. R.; Zhao, Z.; Yorulmaz, S.; Cho, N. J. Self-Assembly Formation of Lipid Bilayer Coatings on Bare Aluminum Oxide: Overcoming the Force of Interfacial Water. *ACS Appl. Mater. Interfaces* **2014**, *7*, 959–968.
(49) Bailey, C. M.; Kamaloo, E.; Waterman, K. L.; Wang, K. F.; Nagarajan, R.; Camesano, T. A. Size Dependence of Gold Nanoparticle Interactions with a Supported Lipid Bilayer: A QCM-D Study. *Biophys. Chem.* **2015**, *203,* 51–61.
(50) Wargenau, A.; Tufenkji, N. Direct Detection of the Gel–Fluid Phase Transition of a Single Supported Phospholipid Bilayer Using Quartz Crystal Microbalance with Dissipation Monitoring. *Anal. Chem.* **2014**, *86*, 8017–8020.
(51) Sauerbrey, G. Verwendung von Schwingquarzen zur Wägung dünner Schichten und zur Mikrowägung. *Z. Phys.* **1959**, *155*, 206–222.
(52) Kunze, A.; Zhao, F.; Marel, A. K.; Svedhem, S.; Kasemo, B. Ion-mediated Changes of Supported Lipid Bilayers and Their Coupling to the Substrate. A Case of Bilayer Slip? *Soft Matter* **2011**, *7*, 8582–8591.
(53) Dukhin, A. S.; Goetz, P. J. (Eds.). *Ultrasound for Characterizing Colloids–Particle Sizing, Zeta Potential, Rheology*; Studies in Interface Science Series 15; Elsevier, 2002; p 249.
(54) Cuddy, M. F.; Poda, A. R.; Brantley, L. N. Determination of Isoelectric Points and the Role of pH for Common Quartz Crystal Microbalance Sensors. *ACS Appl. Mater. Interfaces* **2013**, *5,* 3514–3518.
(55) Leroueil, P. R.; Berry, S. A.; Duthie, K.; Han, G.; Rotello, V. M.; McNerny, D. Q.; Banaszak Holl, M. M. Wide Varieties of Cationic Nanoparticles Induce Defects in Supported Lipid Bilayers. *Nano Lett.* **2008**, *8*, 420–424.
(56) Li, W.; Liu, D.; Wu, J.; Kim, C.; Fortner, J. D. Aqueous Aggregation and Surface Deposition Processes of Engineered Superparamagnetic Iron Oxide Nanoparticles for Environmental Applications. *Environ. Sci. Technol.* **2014**, *48*, 11892–11900.
(57) Guleryuz, H.; Kaus, I.; Buron, C. C.; Filiâtre, C.; Hedin, N.; Bergström, L.; Einarsrud, M. A. Deposition of Silica Nanoparticles onto Alumina Measured by Optical Reflectometry and Quartz Crystal Microbalance with Dissipation Techniques. *Colloids Surf., A* **2014**, *443*, 384–390.
(58) Vishwanath, K.,; Zhong, W.; Close, M.; Mycek, M. A. Fluorescence quenching by polystyrene microspheres in UV-visible and NIR tissue-simulating phantoms. *Opt. Express* **2006,** *14*, 7776–7788.
(59) Nakashima, K.; Kido, N. Fluorescence Quenching of 1-Pyrenemethanol by Methylviologen in Polystyrene Latex Dispersions. *Photochem. Photobiol.* **1996**, *64*, 296–302.

(60) Xiao, X.; Montaño, G. A.; Edwards, T. L.; Allen, A.; Achyuthan, K. E.; Polsky, R.; Brozik, S. M. Surface Charge Dependent Nanoparticle Disruption and Deposition of Lipid Bilayer Assemblies. *Langmuir* **2012**, *28*, 17396–17403.

TOC Graphic Art